

One-Shot GAN: Learning to Generate Samples from Single Images and Videos

Vadim Sushko

Bosch Center for Artificial Intelligence
vadim.sushko@bosch.com

Jürgen Gall

University of Bonn
gall@iai.uni-bonn.de

Anna Khoreva

Bosch Center for Artificial Intelligence
anna.khoreva@bosch.com

Training video & generated samples from a single video



Training image & generated samples from a single image



Figure 1: One-Shot GAN images generated from a single video or a single image. Our model successfully operates in different one-shot settings, including learning from a single video (first two rows) or a single image (last three rows), generating new scene compositions with varying content and layout. For example, from the single training video with a car on the road, One-Shot GAN generates images without a car or with two cars; for the single air balloon image, it can synthesize layouts with a different number and position of the balloons in the scene. (Original samples are shown in grey or red frames.)

Abstract

Given a large number of training samples, GANs can achieve remarkable performance for the image synthesis task. However, training GANs in extremely low-data regimes remains a challenge, as overfitting often occurs, leading to memorization or training divergence. In this work, we introduce One-Shot GAN, an unconditional generative model that can learn to generate samples from a single training image or a single video clip. We propose a two-branch discriminator architecture, with content and layout

branches designed to judge internal content and scene layout realism separately from each other. This allows synthesis of visually plausible, novel compositions of a scene, with varying content and layout, while preserving the context of the original sample. Compared to previous single-image GAN models, One-Shot GAN generates more diverse, higher quality images, while also not being restricted to a single image setting. We show that our model successfully deals with other one-shot regimes, and introduce a new task of learning generative models from a single video.

1. Introduction

The quality of synthetic images produced by generative adversarial networks (GANs) [7] has greatly improved in recent years [50, 4, 30, 17, 32, 23, 34, 18]. These impressive results are in large part enabled by the availability of large, diverse datasets, typically consisting of tens of thousands of images. This dependency on the availability of training data limits the applicability of GANs in domains where collecting a large dataset is not feasible. In some real-world applications, collection of even a small dataset remains challenging due to specific constraints related to privacy, copyright status, subject type, geographical location, time, and dangerous or hazardous environments. It may happen that rare objects or events are present only in one image or video, and it is difficult to obtain a second one. For example, this includes images of exclusive artworks or videos of traffic accidents recorded in extreme conditions. Enabling GANs to learn in such *one-shot* scenarios thus has the potential to improve their utilization in practice.

Prior work [36, 35, 9] studied one-shot image synthesis in the context of learning from a *single image* (Fig. 1, rows 3-5). In this work, we introduce a new one-shot setting: learning to synthesize images from a *single video* (Fig. 1, rows 1-2), where the training data is a collection of frames from a 2-10 second video clip. In practice, capturing such a short video takes almost as little effort as collecting one image. However, compared to a single image, a video contains much more information about the scene and the objects of interest (e.g., different poses and locations of objects, various camera views, dynamic backgrounds). Learning from a video can enable synthesis of higher quality, more diverse images, while still operating in a one-shot mode, and therefore can improve its usability for practical applications.

Training GANs in a low-data regime is challenging as the models are prone to overfitting, leading to memorization of training data or poor synthesis quality due to training instability [16, 24]. To mitigate overfitting, recent single-image GAN models [35, 9] proposed to learn an internal patch-based distribution of an image, employing a cascade of multi-scale patch-GANs [13] trained in multiple stages. Though these models overcome memorization, producing different versions of a training image, they cannot learn high-level semantic properties of the scene, e.g., to dissect objects from the background. They often suffer from incoherent shuffling of image patches, distorting objects and producing unrealistic layouts (see Fig. 4 and 5). Other low-data GANs, such as FastGAN [24], have memorization problems when applied in the one-shot setting (see Sec. 4).

We aim to go beyond patch-based learning, seeking to generate novel, plausible compositions of objects in the scene, while preserving the original image context. We want to learn a one-shot model which is able to compose new layouts, re-arrange objects in the scene, remove or du-

plicate instances, and change their shape and size. The new compositions should be visually plausible, with objects preserving their appearance and natural shape, and scene layouts looking realistic to the human eye. Reaching such synthesis quality in a one-shot setting is notably challenging, as the model needs to learn to distinguish objects and background using only a single image or video for training, without any direct object supervision (e.g. mask annotations).

To this end, we introduce One-Shot GAN, an unconditional, single-stage GAN model, capable of generating images that are substantially different from the original training sample, while still preserving its context. This is achieved by two key ingredients: the novel discriminator design and the proposed diversity regularization for the generator. Our discriminator has two branches, separately judging image content and scene layout realism. The content branch evaluates objects' fidelity irrespective of their spatial arrangement, while the layout branch looks only at the global scene coherency. Disentangling the discriminator's decision about content and layout helps to prevent overfitting and provides a more informative signal to the generator. To achieve a high diversity among generated samples, we further extend the regularization technique of [48] to one-shot unconditional image synthesis. The prior work of [48] encourages the generation of different images depending on their input latent codes, thus the difference between images is proportional to the distance between their codes in the latent space. Assuming that in the one-shot setting all generated images should belong to one semantic domain (i.e. preserve the original training sample context), and thus should be more or less equally different from each other, we apply diversity regularization uniformly, independent of the latent space distance. Moreover, we use the regularization in the feature space, inducing both high- and low-level diversity.

We demonstrate the effectiveness of our model for the single image setting as well as for the novel single video setting in Sec. 4. One-Shot GAN is the first model that successfully learns in both of these one-shot settings, improving over prior work [35, 9, 24] on both image quality and diversity. In contrast to FastGAN [24], our model does not suffer from memorization (see Table 1 and 2); compared to single-image GANs [35, 9], our model does not distort objects, preserving their appearance. In summary, our contributions are: 1) We propose a new one-shot task of learning generative models from a single video. 2) We present a novel two-branch discriminator, encouraging the generation of images with scene layouts and content substantially different from training samples. Our proposed diversity regularization ensures a high variability among generated samples in the challenging one-shot image synthesis setting. 3) With One-Shot GAN, we universally achieve high quality and diversity when learning from both single images and videos, outperforming prior work on two different datasets.

2. Related Work

Single Image Generative Models. Several works have investigated learning generative models from a single image. [43, 37] showed that when trained on a single image, a deep convolutional network can learn a useful representation that captures the internal statistics of that image. These learned representations can be employed to synthesize textures from a sample texture image [14, 3, 41, 55, 21, 42], to "blindly" super-resolve [37, 2, 25], or to inpaint the image [43]. Recently, single image GAN models [36, 35] have been proposed, revealing the power of image priors learned from a single natural image for synthesis and manipulation tasks. InGAN [36] introduced a GAN model conditioned on a single natural image, which can remap the input to any size or shape while preserving its internal patch-based distribution. SinGAN [35] employed an unconditional GAN to produce images of arbitrary size from noise, and used a multi-stage training scheme to learn the multi-scale patch distribution of an image. ConSinGAN [9] extended SinGAN by improving the rescaling for multi-stage training and training several stages concurrently, which enabled reducing the size of the model and making the training more efficient. To explore the semantic meaning of patches inside a single image, [22] used a conditional single image GAN with the segmentation map as dense conditional input.

Contrary to single image GANs [35, 9], our model is trained in a single stage, and is designed to learn not only the internal patch-based distribution of an image, but also to capture high-level content, such as scene layouts or appearance of objects. The latter enables more diverse, higher-quality synthesis (see Table 1). Our model is also more universal: it effectively operates in different low-data regimes, learning from a single image or a single video, and thus can be applied to a wider range of real-world scenarios.

Few-Shot Generative Models. Few-shot image generation seeks to generate more data of a given domain, with only a few training samples available. Many existing methods resorted to train a conditional GAN using large image sets of seen classes, and then used it to generate new images for an unseen class based on a few examples [10, 1, 11]. [1] injected random noise into the generator conditioned on an image to produce a slightly different sample from the same class. [12, 11] proposed to fuse the information from multiple conditional images of the same class. Others focused on improving the sample efficiency of GANs by few-shot adaptation [27, 44, 33, 45, 28]. These methods usually start from GANs pre-trained on large datasets, and adapt them on a few samples in the target domain by fine-tuning all weights of the generator and discriminator [45], freezing lower discriminator layers [27], changing batch statistics [28], restricting the space of trainable parameters [33], and transferring the knowledge via a miner network [44]. Unlike our work, the above methods heavily rely on *exter-*

nal knowledge from a pre-trained GAN, and their performance highly depends on the semantic consistency between the target domain and the pre-trained model. In practice, there is no guarantee that a compatible pre-training dataset is available, and pre-training on semantically incompatible samples might lead to an even worse performance [51].

Another line of work focused on improving the stability of GANs when trained with limited data. To prevent the discriminator from overfitting, [16, 53, 51] explored different data augmentations for both real and generated images. Similarly, we employ both image and feature augmentations during training to improve diversity of the generated samples while operating in one-shot mode. Most recently, FastGAN [24] has proposed to train an unconditional GAN model for few-shot image synthesis from scratch. To avoid overfitting and mode-collapse, they enabled a fast learning of the generator through a skip-layer channel-wise excitation module, and used a self-supervised discriminator to continuously provide useful signals to the generator. However, to achieve good results, FastGAN requires a sufficient number of training samples (~ 100), while One-Shot GAN successfully learns even from only one image (see Sec. 4.1).

3. One-Shot GAN

In this section, we present One-Shot GAN, an unconditional GAN model that can work in different one-shot regimes (learning from one image or one video) and can generate new plausible compositions of a given scene with varying content and layout. The key ingredients of One-Shot GAN are a novel design of a two-branch discriminator (Sec. 3.1) and a diversity regularization technique introduced for one-shot image synthesis (Sec. 3.2).

3.1. Content-Layout Discriminator

One challenge of training GANs in the one-shot setting is the problem of overfitting to the original sample. In many cases the model can simply memorize the original training image and its augmented versions (if used during the training). To avoid this memorization effect, [35, 9] proposed to learn an internal patch-based distribution by using a hierarchy of patch-GANs [13, 21] at different image scales. As the employed patch-GANs have small receptive fields and limited capacity, they are prevented from memorizing the full image. However, the downside of training each scale of the patch-GANs in a separate stage is that any layout decisions made by the coarser scale generators cannot be corrected at later, finer generation stages. Thus, both the quality and diversity of generated images are highly dependent on the chosen lowest resolution size. This parameter needs careful tuning for specific images at hand, as otherwise image layouts may exhibit lack of diversity or loss of global coherency (see Fig. 3). Moreover, this approach does not generalize to a single video setting (see Table 2 and Fig. 5).

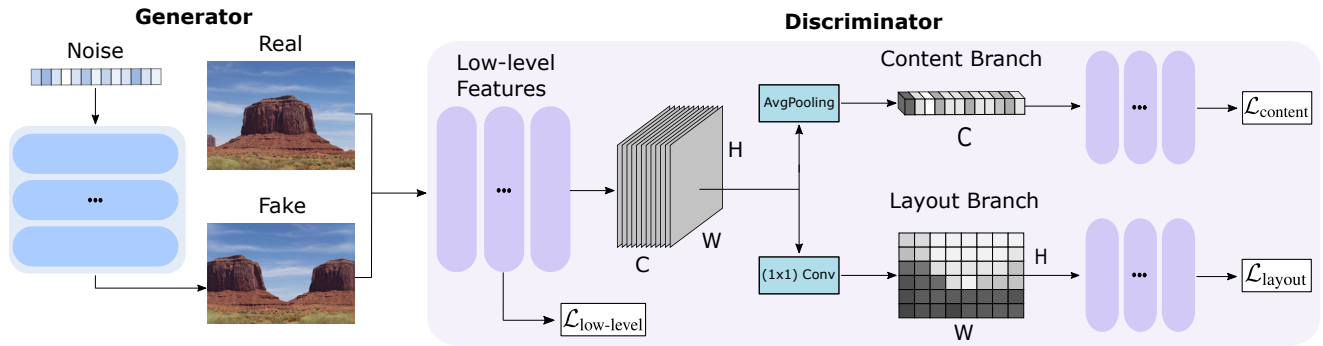


Figure 2: One-Shot GAN. The two-branch discriminator judges the content distribution separately from the scene layout realism and thus enables the generator to produce images with varying content and global layouts. See Sec. 3.1 for details.



Figure 3: Limitation of the multi-stage training of single image patch-GAN methods. As the finer generation stages cannot correct the layout decision made by the coarser scale generators, without a careful tuning of the lowest resolution size the model falls into producing images with very low diversity (first row) or lacking global coherency (last row).

We therefore introduce an alternative solution to overcome the memorization effect but still produce high-quality images. We note that in order to produce realistic and diverse images, the generator should learn the appearance of objects and combine them in the image in a globally-coherent way. To this end, we propose a discriminator that judges the *content* distribution of a given image separately from its *layout* realism. To achieve the disentanglement, we design a two-branch discriminator architecture, with separate content and layout branches. Note that the branching of the discriminator happens after intermediate layers; this is done in order to learn relevant representations for building the branches. As seen from Fig. 2, our discriminator consists of the low-level feature extractor $D_{low-level}$, the content branch $D_{content}$, and the layout branch D_{layout} . For a given image x , the purpose of $D_{low-level}$ is to learn low-level features and to produce an image representation $F(x) = D_{low-level}(x)$ for the branches. Next, $D_{content}$ will judge the content of $F(x)$, irrespective from its spatial layout, while on the other hand D_{layout} will inspect only the spatial information extracted from $F(x)$. Inspired by the attention modules of [29, 47], we implement the content-layout disentanglement by squeezing channels or spatial di-

mensions of the intermediate features $F(x)$. Note that afterwards the branches $D_{content}$ and D_{layout} receive only limited information about the image from $F(x)$, preventing them from overfitting to the whole image, and thus mitigating the negative effect of memorizing the original image.

Content branch. The content branch decision should be based upon the image content, i.e., the fidelity of objects composing the image, independent of their spatial location in the scene layout. Let the feature map $F(x)$ have dimensions $H \times W \times C$, where H, W, C are the height, width and channels of the feature map. Note that the spatial resolution $H \times W$ captures spatial information, while the channels C encode the semantic representation. As we want the content branch to ignore the spatial information, we aggregate the spatial information $H \times W$ across the channels C . We do so by applying global average pooling, forming a feature map $F_{content}(x)$ with size $1 \times 1 \times C$, which is then processed by several layers for further real/fake decision making. By removing the spatial information, $D_{content}(x)$ is induced to respond to content features encoded in different channels regardless of their spatial location.

Layout branch. The layout branch decision should be based upon the spatial location of objects in the scene, but not their specific appearance. Thus, in contrast to the content branch, the layout branch is designed to judge only the spatial information of the feature map $F(x)$, filtering out the content details. Since the layout information is encoded only in spatial dimensions $H \times W$, and not in channels C , we aggregate the channel information from $F(x)$ via a (1×1) convolution with only one output channel, which forms a feature map $F_{layout}(x)$ with size $H \times W \times 1$. This channel aggregation weakens the content representation but does not affect the spatial information. The $F_{layout}(x)$ features are further processed by several layers before a real/fake decision is made. As $D_{layout}(x)$ is designed to be sensitive only to the spatial representation of the input image, it learns to judge the realism of scene layouts.

Feature augmentation. The proposed two-branch discriminator prevents the memorization of training samples,

enabling the generation of images with a different content and a different layout from the original sample. To further improve the diversity of generated images, we propose to augment the content $F_{content}(x)$ and layout $F_{layout}(x)$ features of real images. For the single image setting this is done by mixing the features of two different augmentations of the original image, and for the single video setting by mixing the features of augmentations of two different video frames. For two real samples x_1 and x_2 we apply a mixing transformation $F_*(x_1) = T_{mix}(F_*(x_1), F_*(x_2))$. We use two types of mixing: 1) For the layout branch, we sample a rectangular crop of $F_{layout}(x_2)$ and paste it on to $F_{layout}(x_1)$ at the same spatial location, similarly to CutMix [49]. In contrast to CutMix, our approach augments features, not input images, and mixes only features of real images. 2) For the content branch, we sample a set of channels from $F_{content}(x_2)$ and copy their values to the corresponding channels of $F_{content}(x_1)$. As the channels encode semantic features of images, we expect the resulting augmented tensor to represent objects observed in two different images. We also found it useful to remove channels from $F_{content}(x)$, thus removing some object representations. For this, we sample a set of channels and drop out their values [38, 40]. With the above augmentations, $D_{content}$ and D_{layout} see significantly more variance in both the content and layout representations of real images, which prevents overfitting and improves the diversity of generated samples. The feature augmentation (FA) effect is shown in Table 3.

Adversarial loss. To evaluate images at different scales, we design our discriminator to make a binary true/false decision at each intermediate resolution. For each discriminator part D_* : $D_{low-level}$, $D_{content}$, and D_{layout} , the loss is computed by aggregating the contributions across all layers constituting the corresponding discriminator part:

$$\mathcal{L}_{D_*} = \frac{1}{N_*} \sum_{l=1}^{N_*} \mathcal{L}_{D_*^l}, \quad (1)$$

where D_*^l is the l -th ResNet block of D_* , N_* is the number of ResNet blocks used in D_* , and the loss $\mathcal{L}_{D_*^l}$ is the binary cross-entropy: $\mathcal{L}_{D_*^l} = \mathbb{E}_x[\log D_*^l(x)] + \mathbb{E}_z[\log(1 - D_*^l(G(z)))]$. D_*^l aims to distinguish between real x and generated $G(z)$ images based on their corresponding features at block l , which captures either their low-level details, content, or layout at a certain resolution. The overall adversarial loss for One-Shot GAN is then computed by taking the decisions from the content branch $D_{content}$, the layout branch D_{layout} , and the low-level features of $D_{low-level}$:

$$\mathcal{L}_{adv}(G, D) = \mathcal{L}_{D_{content}} + \mathcal{L}_{D_{layout}} + 2\mathcal{L}_{D_{low-level}}, \quad (2)$$

where D aims to distinguish between real and generated images based on their low-level, content, and layout realism. As the two branches of the discriminator operate on high-level image features, contrary to only one $D_{low-level}$

operating on low-level features, we double the weighting for the $\mathcal{L}_{D_{low-level}}$ loss term. This is done in order to properly balance the contributions of different feature scales and encourage the generations of images with good low-level details, plausible content, and coherent scene layouts.

3.2. Diversity Regularization

To improve the variability among the generated image samples, we propose to add a diversity regularization (DR) loss term \mathcal{L}_{DR} to the One-Shot GAN objective. In prior work [48, 52, 5] also proposed to use diversity regularization for GAN training, but mainly to avoid mode collapse, and assuming the availability of a large training set. The regularization of [48] aimed to encourage the generator to produce different outputs depending on the input latent code, in such a way that generated samples with closer latent codes should look more similar to each other, and vice versa. In contrast, our diversity regularization is tuned for one-shot image synthesis. Assuming that in the one-shot mode we are operating in one semantic domain, the generator should produce images that are in-domain but more or less equally different from each other, and substantially different from the original training sample. In the one-shot synthesis setting, the perceptual distance of the generated images should not be dependent on the distance between their latent codes. Thus, we propose to encourage the generator to produce perceptually different image samples independent of their distance in the latent space. Mathematically, the new diversity regularization is expressed as:

$$\mathcal{L}_{DR}(G) = \mathbb{E}_{z_1, z_2} \left[\frac{1}{L} \sum_{l=1}^L \|G^l(z_1) - G^l(z_2)\| \right], \quad (3)$$

where $\|\cdot\|$ denotes the $L1$ norm, $G^l(z)$ indicates a feature extracted after l -th resolution block of the generator G given input z , and z_1, z_2 are randomly sampled latent codes in the batch, i.e. $z_1, z_2 \sim N(0, 1)$. By regularizing the generator to maximize Eq. 3, we force the generator to produce diverse outputs for different latent codes z . Note that, in contrast to [48, 52, 5], we compute the distance between samples in the feature space of the generator. Computing the distance in the feature space results in more meaningful diversity among the generated images, as different layers of the generator capture different image semantics, inducing both high-level and low-level diversity. Computing the distance in the image space directly from the generator outputs, i.e. $\mathcal{L}_{DR}(G) = \|G(z_1) - G(z_2)\|$ as in [5], leads to reduced image diversity in our experiments (see Table 4).

The overall One-Shot GAN objective can be written as:

$$\min_G \max_D \mathcal{L}_{adv}(G, D) - \lambda \mathcal{L}_{DR}(G), \quad (4)$$

where λ controls the strength of the diversity regularization and \mathcal{L}_{adv} is the adversarial loss in Eq. 2. The proposed diversity regularization is shown to be highly-effective for

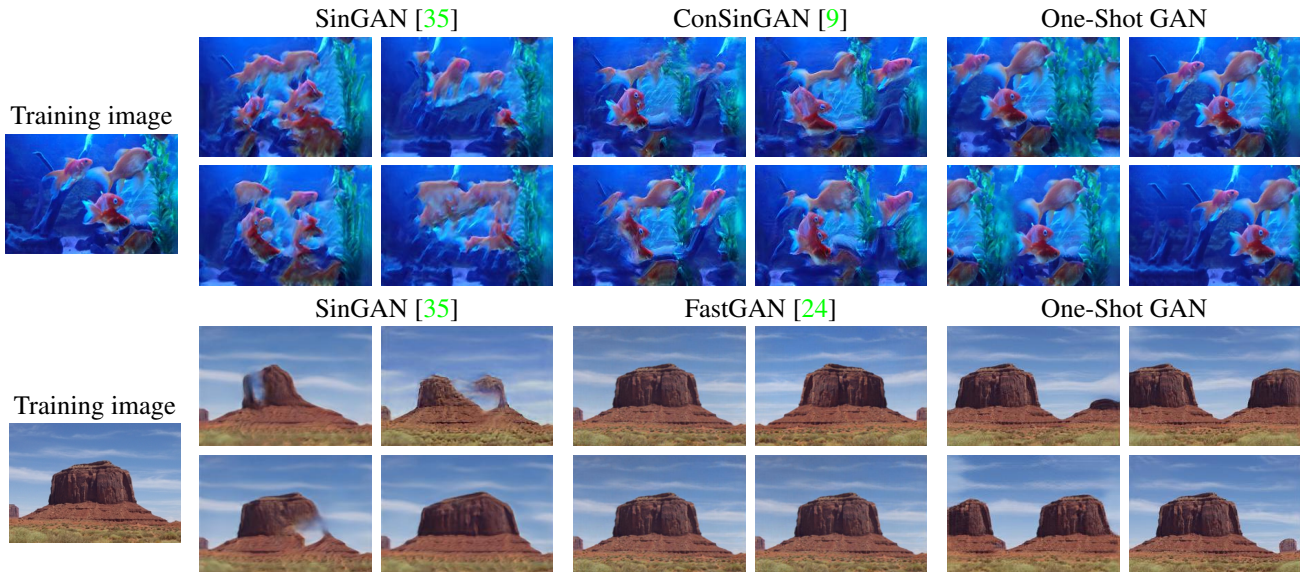


Figure 4: Comparison in the Single Image setting. Single-image GANs of [35, 9] may incoherently shuffle patches (e.g. sky textures below horizon, perturbed fish contours), and few-shot FastGAN [24] reproduces the original image or its flipped version. In contrast, One-Shot GAN achieves high diversity, preserves content distribution, and maintains realistic layouts.

Method	Places [54]						DAVIS-YFCC100M [31, 39]					
	SIFID [35]		LPIPS↑	MS-SSIM↓	Pixel↑ Diversity	Dist. to train	SIFID [35]		LPIPS↑	MS-SSIM↓	Pixel↑ Diversity	Dist. to train
	best↓	mean↓					best	mean				
SinGAN [35]	0.09	0.15	0.22	0.75	0.52	0.24	0.10	0.13	0.26	0.69	0.54	0.30
ConSinGAN [9]	0.06	0.08	0.24	0.73	0.50	0.25	0.08	0.09	0.29	0.65	0.59	0.31
FastGAN [24]	0.11	0.14	0.15	0.81	0.48	0.08	0.10	0.13	0.18	0.77	0.49	0.11
One-Shot GAN	0.05	0.06	0.28	0.67	0.57	0.31	0.07	0.08	0.33	0.63	0.66	0.37

Table 1: Comparison with other methods in the Single Image setting on Places [54] and DAVIS-YFCC100M [31, 39] datasets.

One-Shot GAN, while prior diversity regularizations [48, 52, 5] underperform (see Sec. 4.2 and Table 4).

3.3. Implementation and Training

The One-Shot GAN generator consists of ResNet blocks, similar to BigGAN [4]. However, we do not employ Batch-Norm or self-attention. Following MSG-GAN [15], we generate images at higher-resolution intermediate scales, passing them to $D_{low-level}$ in order to facilitate the gradient flow from the discriminator. The latent vector z , of dimensionality 64, is sampled from $N(0, 1)$. For the diversity regularization we use the tanh nonlinearity on the features from the final convolutions of the generator blocks.

The One-Shot GAN discriminator also uses ResNet blocks. We set $N_{low-level} = 3$, $N_{layout} = N_{content} = 4$, thus using 3 ResNet blocks before branching and 4 ResNet blocks for the content and layout branches. To enable multi-scale gradients, we incorporate images at different scales using the $\phi_{lin-cat}$ strategy from [15]. The proposed feature augmentation (FA) is applied with probability 0.4 at every discriminator forward pass. We additionally employ standard image augmentation strategies [20] for the discriminator training. Following [16, 53], we augment both real and fake images; with a probability of 0.7 for each forward pass,

we apply translation, random cropping, image rotation, and horizontal flipping. In alignment with [16], we observe no signs of leaking augmentations in the generated samples.

In contrast to previous single image GANs [35, 9], which employ a multi-stage training scheme, One-Shot GAN is trained end-to-end in one stage with the losses from Eq. 4, where $\lambda = 0.15$ for \mathcal{L}_{DR} . We use spectral normalization [26] for both G and D , and do not use a reconstruction loss as in [35, 9], or any other stabilization techniques. One-Shot GAN is trained using the ADAM optimizer [19] with $(\beta_1, \beta_2) = (0.5, 0.999)$, a learning rate of 0.0002 for both G and D , and a batch size of 5 (using different augmentations of a single image or video frames).

4. Experiments

We evaluate One-Shot GAN on two different one-shot settings: Single Image and Single Video, using the same model configuration described in Sec. 3.3. We train it for 100k iterations on an image and 300k iterations on a video.

Datasets. Following [35], we evaluate the Single Image setting on 50 images from Places [54]. In addition to their protocol, we select 15 videos from the DAVIS [31] and YFCC100M [39] datasets. In the Single Video setting, we



Figure 5: Comparison with other methods in the Single Video setting. While other models fall into reproducing the training frames or fail to draw objects, One-Shot GAN generates high-quality images substantially different from the original frames.

Method	SIFID ↓		LPIPS ↑	MS-SSIM ↓	Dist. to train
	$\frac{H \times W}{4}$	$\frac{H \times W}{16}$			
SinGAN [35]	2.47	96.35	0.32	0.65	0.51
ConSinGAN [9]	2.74	74.50	0.34	0.62	0.53
FastGAN [24]	0.79	9.24	0.43	0.55	0.13
One-Shot GAN	0.55	5.14	0.43	0.54	0.34

Table 2: Comparison in the Single Video setting.

use all the frames as training images, while for the Single Image setup we use only one middle frame. The chosen videos last for 2-10 seconds and consist of 60-100 frames.

Metrics. To assess the quality of generated images, we measure the single FID (SIFID) [35]. Its original formulation uses InceptionV3 features before the first pooling layer at a spatial resolution of $\frac{H \times W}{4}$, which capture low-level image details. To assess high-level properties, such as scene layouts, we also propose to compute SIFID at higher-level features, at a resolution of $\frac{H \times W}{16}$. To measure the diversity of generated samples, we adopt the pixel diversity metric from [35]. To measure perceptual and structural diversity, we also report the average LPIPS [6] and MS-SSIM [46] across pairs of generated images. To verify that the models do not simply reproduce the training set, we report average LPIPS to the nearest image in the training set, augmented in the same way as during training (Dist. to train). We note that SIFID tends to penalize diversity, favouring overfitting [33]. Thus, to account for this quality-diversity trade-off, a fair analysis should assess both diversity and quality.

Comparison models. We compare our model with single image methods, SinGAN [35] and ConSinGAN [9], and with a recent model on few-shot image synthesis, FastGAN [24]. We use the original implementation codes provided by the authors. While training single image GANs from [35, 9] on a single video, we applied the reconstruction loss on all frames, as we found this helpful in stabilizing the training.

4.1. Main results

Tables 1 and 2 present a quantitative comparison between the models in the Single Image and Single Video settings, while the respective visual results are shown in Fig. 4 and 5. As seen from the tables, One-Shot GAN notably outperforms other models in both studied settings. Despite a potential trade-off between quality and diversity, our model achieves better performance in both, reaching lower SIFID values and higher diversity scores. Importantly, only One-Shot GAN successfully learns from both single images and videos, generating globally-coherent images of high diversity. Next, we analyse results in these settings separately.

Single Image. As seen from Fig. 1 and 4, in the Single Image setting, One-Shot GAN produces diverse, high-quality samples. For example, our model can change the number and placement of balloons in the sky, or edit the contour and position of rocks in the desert. Note that such changes retain the appearance of objects, preserving original context, and maintain scene layout realism. In contrast, the prior single image GANs, SinGAN and ConSinGAN, disturb the appearance of objects (e.g. by washing away fish contours) and disrespect layouts (e.g. sky textures appear below the horizon), while having modest diversity. This is reflected in their higher SIFID and lower diversity scores in Table 1. The few-shot FastGAN model suffers from memorization, reproducing the training image or its flipped version. In Table 1 this is reflected in lowest diversity and Dist. to train (in red) metrics on both datasets. Despite having the lowest diversity, we observe that FastGAN does not reach a low SIFID due to leaking augmentations (horizontal flipping).

Single Video. In the Single Video setting, there is much more information to learn from, and generative models can consequently learn more interesting combinations of objects and scenes. Fig. 1 and 5 show the images generated by

Method	Single Image						Single Video				
	SIFID ↓		LPIPS ↑	MS-SSIM ↓	Pixel ↑	Dist.	SIFID ↓		LPIPS ↑	MS-SSIM ↓	Dist.
	$\frac{H \times W}{4}$	$\frac{H \times W}{16}$					$\frac{H \times W}{4}$	$\frac{H \times W}{16}$			
Full model	0.08	16.30	0.33	0.63	0.66	0.37	0.55	5.14	0.43	0.54	0.34
No Layout br.	0.14	20.29	0.35	0.60	0.67	0.40	0.71	11.70	0.42	0.54	0.38
No Content br.	0.08	23.25	0.34	0.62	0.64	0.36	0.73	10.43	0.41	0.55	0.33
No branches	0.03	7.73	0.13	0.84	0.43	0.12	0.42	3.73	0.37	0.59	0.18
No DR	0.05	11.99	0.04	0.95	0.33	0.06	0.40	9.81	0.30	0.68	0.32
No FA	0.08	14.81	0.27	0.68	0.58	0.33	0.51	4.85	0.41	0.56	0.32
No $\mathcal{L}_{D_{low-level}}$	0.08	15.92	0.27	0.70	0.56	0.29	0.58	5.32	0.40	0.56	0.31

Table 3: Ablation study on proposed modifications on DAVIS-YFCC100M in the Single Image and Video settings. Indicators of collapsed diversity (low LPIPS, Pixel Diversity, high MS-SSIM) or poor quality (high SIFID) are marked in red.

Regularization	SIFID ↓	LPIPS ↑	MS-SSIM ↓	Pixel ↑
				Diversity
None	0.05	0.04	0.95	0.33
zCR [52]	0.05	0.06	0.93	0.37
DS [48]	0.06	0.14	0.84	0.45
DR (im. space)	0.07	0.21	0.72	0.52
DR	0.08	0.33	0.63	0.66

Table 4: Comparison of diversity regularizations in the Single Image setting on DAVIS-YFCC100M [31, 39].

One-Shot GAN in this setting. Our model generates high-quality images that are substantially different from the training frames, adding/removing objects and changing scene geometry. For example, having seen a car following a road (Fig. 1), One-Shot GAN generates the scene without a car or with two cars. In Fig. 5 our model varies the length of a bus and placement of trees, or removes a horse from the scene and changes the jumping obstacle configuration. In contrast, SinGAN, tuned to learn from a single image, does not generalize to the Single Video setting, distorting objects and producing unrealistic scene layouts (low diversity and an extremely high SIFID in Table 2). FastGAN, on the other hand, generates images with reasonable fidelity, but fails to produce samples with non-trivial layout changes, having a very low Dist. to train score (0.13 in Table 2). More qualitative results can be found in Sec. F in the suppl. material.

4.2. Ablations

In Table 3 we demonstrate the importance of the proposed modifications. In each line we remove only one model component, starting from our full model. Firstly, we ablate our discriminator architecture, testing it without the layout branch, without the content branch, or without both branches (No branches), corresponding to a standard GAN discriminator. As seen from Table 3, using only one of the branches shows good diversity, but the model fails to generate globally-coherent images, having a high $\frac{H \times W}{16}$ -scale SIFID. The discriminator with no branches, in contrast, memorizes the training images and reproduces them with poor diversity. The qualitative results for these ablation models are presented in Sec. E in the suppl. material. Next,

we observe the effect of the proposed diversity regularization (DR), feature augmentation (FA), and low-level loss $\mathcal{L}_{D_{low-level}}$. Without DR, the model does not achieve multimodality, scoring low on the diversity metrics. The absence of FA notably decreases diversity, which is reflected in the diversity scores dropping by 0.02-0.08 points. Removing $\mathcal{L}_{D_{low-level}}$ also reduces diversity; we discuss this effect in Sec. D in the suppl. material. Overall, we observe that the success of our model in both settings is enabled by both the two-branch discriminator and the diversity regularization.

In Table 4 we compare our DR to the latent consistency regularization (zCR) [52], diversity-sensitive loss (DS) [48] and no regularization (None). We apply zCR only to the generator loss, leaving the discriminator objective intact. As both zCR and DS operate in the image space, we test our proposed DR in the image space instead of the G feature space, as in [5]. As seen from Table 4, our DR noticeably improves over zCR and DS on all diversity metrics. We find it beneficial to use DR in the feature space, which leads to more variation in the generated samples. Interestingly, Table 4 illustrates a quality-diversity trade-off, where improvements in diversity lead to deterioration in SIFID.

5. Conclusion

We propose One-Shot GAN, a new unconditional generative model operating on two different one-shot settings, such as learning from a single image or video. In such low-data regimes, our model prevents memorization and generates diverse images that are significantly different from the training set. Inherently, one-shot image synthesis is constrained by the appearance of objects present in the original sample. Nevertheless, One-Shot GAN can synthesize novel scene compositions by blending objects in different combinations, changing their shape or position in the image, while preserving the original context and plausibility of the scene. Such compositionality is enabled by the model’s ability to distinguish objects and backgrounds, astonishingly, while learning from a single image or video. We believe One-Shot GAN provides a useful tool for data augmentation in domains where data collection remains challenging.

References

- [1] A. Antoniou, A. Storkey, and H. Edwards. Data augmentation generative adversarial networks. In *International Conference on Learning Representations (ICLR)*, 2017. 3
- [2] Sefi Bell-Kligler, Assaf Shocher, and M. Irani. Blind super-resolution kernel estimation using an internal-gan. In *Advances in Neural Information Processing Systems (NeurIPS)*, 2019. 3
- [3] Urs Bergmann, Nikolay Jetchev, and Roland Vollgraf. Learning texture manifolds with the periodic spatial gan. In *International Conference on Machine Learning (ICML)*, 2017. 3
- [4] Andrew Brock, Jeff Donahue, and Karen Simonyan. Large scale GAN training for high fidelity natural image synthesis. In *International Conference on Learning Representations (ICLR)*, 2019. 2, 6, 19, 20
- [5] Yunjey Choi, Youngjung Uh, Jaejun Yoo, and Jung-Woo Ha. Stargan v2: Diverse image synthesis for multiple domains. In *Conference on Computer Vision and Pattern Recognition (CVPR)*, 2020. 5, 6, 8
- [6] Alexey Dosovitskiy and Thomas Brox. Generating images with perceptual similarity metrics based on deep networks. In *Advances in Neural Information Processing Systems (NeurIPS)*, 2016. 7
- [7] Ian Goodfellow, Jean Pouget-Abadie, Mehdi Mirza, Bing Xu, David Warde-Farley, Sherjil Ozair, Aaron Courville, and Yoshua Bengio. Generative adversarial nets. In *Advances in Neural Information Processing Systems (NeurIPS)*, 2014. 2
- [8] Martin Heusel, Hubert Ramsauer, Thomas Unterthiner, Bernhard Nessler, and Sepp Hochreiter. GANs trained by a two time-scale update rule converge to a local nash equilibrium. In *Advances in Neural Information Processing Systems (NeurIPS)*, 2017. 11
- [9] Tobias Hinz, Matthew Fisher, Oliver Wang, and Stefan Wermter. Improved techniques for training single-image gans. In *Winter Conference on Applications of Computer Vision (WACV)*, 2021. 2, 3, 6, 7, 11, 12, 15, 19
- [10] Y. Hong, Li Niu, J. Zhang, Jing Liang, and L. Zhang. Deltagan: Towards diverse few-shot image generation with sample-specific delta. *arXiv preprint arXiv:2009.08753*, 2020. 3
- [11] Y. Hong, Li Niu, J. Zhang, Weijie Zhao, Chen Fu, and L. Zhang. F2gan: Fusing-and-filling gan for few-shot image generation. In *ACM International Conference on Multimedia*, 2020. 3
- [12] Y. Hong, Jianfu Zhang, Li Niu, and L. Zhang. Matchinggan: Matching-based few-shot image generation. In *International Conference on Multimedia and Expo (ICME)*, 2020. 3
- [13] Phillip Isola, Jun-Yan Zhu, Tinghui Zhou, and Alexei A Efros. Image-to-image translation with conditional adversarial networks. In *Conference on Computer Vision and Pattern Recognition (CVPR)*, 2017. 2, 3
- [14] Nikolay Jetchev, Urs Bergmann, and Roland Vollgraf. Texture synthesis with spatial generative adversarial networks. *arXiv preprint arXiv:1611.08207*, 2016. 3
- [15] Animesh Karnewar and Oliver Wang. Msg-gan: multi-scale gradient gan for stable image synthesis. In *Conference on Computer Vision and Pattern Recognition (CVPR)*, 2020. 6, 19, 20
- [16] Tero Karras, Miika Aittala, Janne Hellsten, S. Laine, J. Lehtinen, and Timo Aila. Training generative adversarial networks with limited data. In *Advances in Neural Information Processing Systems (NeurIPS)*, 2020. 2, 3, 6
- [17] Tero Karras, Samuli Laine, and Timo Aila. A style-based generator architecture for generative adversarial networks. In *Conference on Computer Vision and Pattern Recognition (CVPR)*, 2019. 2
- [18] Tero Karras, Samuli Laine, Miika Aittala, Janne Hellsten, Jaakko Lehtinen, and Timo Aila. Analyzing and improving the image quality of StyleGAN. In *Conference on Computer Vision and Pattern Recognition (CVPR)*, 2020. 2
- [19] Diederik P. Kingma and Jimmy Ba. Adam: A method for stochastic optimization. In *International Conference on Learning Representations (ICLR)*, 2015. 6, 20
- [20] Alex Krizhevsky, Ilya Sutskever, and Geoffrey E Hinton. Imagenet classification with deep convolutional neural networks. In *Advances in Neural Information Processing Systems (NeurIPS)*, 2012. 6
- [21] Chuan Li and M. Wand. Precomputed real-time texture synthesis with markovian generative adversarial networks. In *European Conference on Computer Vision (ECCV)*, 2016. 3
- [22] Jiacheng Li, Z. Xiong, D. Liu, X. Chen, and Z. Zha. Semantic image analogy with a conditional single-image gan. In *ACM International Conference on Multimedia*, 2020. 3
- [23] Chieh Hubert Lin, Chia-Che Chang, Yu-Sheng Chen, Da-Cheng Juan, Wei Wei, and Hwann-Tzong Chen. Coco-gan: Generation by parts via conditional coordinating. In *International Conference on Computer Vision (ICCV)*, 2019. 2
- [24] Bingchen Liu, Yizhe Zhu, Kunpeng Song, and Ahmed Elgammal. Towards faster and stabilized gan training for high-fidelity few-shot image synthesis. In *International Conference on Learning Representations (ICLR)*, 2021. 2, 3, 6, 7, 11, 12, 14, 16
- [25] Andreas Lugmayr, Martin Danelljan, Luc Van Gool, and Radu Timofte. Srflo: Learning the super-resolution space with normalizing flow. In *European Conference on Computer Vision (ECCV)*, 2020. 3
- [26] Takeru Miyato, Toshiki Kataoka, Masanori Koyama, and Yuichi Yoshida. Spectral normalization for generative adversarial networks. In *International Conference on Learning Representations (ICLR)*, 2018. 6
- [27] Sangwoo Mo, Minsu Cho, and Jinwoo Shin. Freeze discriminator: A simple baseline for fine-tuning gans. In *CVPR AI for Content Creation Workshop*, 2020. 3
- [28] Atsuhiko Noguchi and T. Harada. Image generation from small datasets via batch statistics adaptation. In *International Conference on Computer Vision (ICCV)*, 2019. 3
- [29] Jongchan Park, Sanghyun Woo, Joon-Young Lee, and In So Kweon. Bam: Bottleneck attention module. In *British Machine Vision Conference (BMVC)*, 2018. 4
- [30] Taesung Park, Ming-Yu Liu, Ting-Chun Wang, and Jun-Yan Zhu. Semantic image synthesis with spatially-adaptive normalization. In *Conference on Computer Vision and Pattern Recognition (CVPR)*, 2019. 2

- [31] Jordi Pont-Tuset, Federico Perazzi, Sergi Caelles, Pablo Arbeláez, Alex Sorkine-Hornung, and Luc Van Gool. The 2017 davis challenge on video object segmentation. *arXiv preprint arXiv:1704.00675*, 2017. **6, 8, 11, 20**
- [32] Tingting Qiao, Jing Zhang, Duanqing Xu, and Dacheng Tao. Mirrorgan: Learning text-to-image generation by redescription. In *Conference on Computer Vision and Pattern Recognition (CVPR)*, 2019. **2**
- [33] E. Robb, Wensheng Chu, A. Kumar, and J. Huang. Few-shot adaptation of generative adversarial networks. *arXiv preprint arXiv:2010.11943*, 2020. **3, 7, 11**
- [34] Edgar Schönfeld, Bernt Schiele, and Anna Khoreva. A u-net based discriminator for generative adversarial networks. In *Conference on Computer Vision and Pattern Recognition (CVPR)*, 2020. **2**
- [35] Tamar Rott Shaham, Tali Dekel, and T. Michaeli. Singan: Learning a generative model from a single natural image. In *International Conference on Computer Vision (ICCV)*, 2019. **2, 3, 4, 6, 7, 11, 12, 15, 16, 19, 20**
- [36] Assaf Shocher, S. Bagon, Phillip Isola, and M. Irani. Ingan: Capturing and retargeting the “dna” of a natural image. In *International Conference on Computer Vision (ICCV)*, 2019. **2, 3**
- [37] Assaf Shocher, N. Cohen, and M. Irani. Zero-shot super-resolution using deep internal learning. In *Conference on Computer Vision and Pattern Recognition (CVPR)*, 2018. **3**
- [38] Nitish Srivastava, Geoffrey Hinton, Alex Krizhevsky, Ilya Sutskever, and Ruslan Salakhutdinov. Dropout: A simple way to prevent neural networks from overfitting. *Journal of Machine Learning Research (JMLR)*, 2014. **5**
- [39] Bart Thomee, David A Shamma, Gerald Friedland, Benjamin Elizalde, Karl Ni, Douglas Poland, Damian Borth, and Li-Jia Li. Yfcc100m: The new data in multimedia research. *Communications of the ACM*, 2016. **6, 8, 11**
- [40] Zhengsu Chen Jianwei Niu Qi Tian. Dropfilter: Dropout for convolutions. *arXiv preprint arXiv:1810.09849*, 2018. **5**
- [41] D. Ulyanov, V. Lebedev, A. Vedaldi, and V. Lempitsky. Texture networks: Feed-forward synthesis of textures and stylized images. In *International Conference on Machine Learning (ICML)*, 2016. **3**
- [42] D. Ulyanov, A. Vedaldi, and V. Lempitsky. Improved texture networks: Maximizing quality and diversity in feed-forward stylization and texture synthesis. In *Conference on Computer Vision and Pattern Recognition (CVPR)*, 2017. **3**
- [43] D. Ulyanov, A. Vedaldi, and V. Lempitsky. Deep image prior. In *Conference on Computer Vision and Pattern Recognition (CVPR)*, 2018. **3**
- [44] Yaxing Wang, Abel Gonzalez-Garcia, David Berga, L. Herranz, F. Khan, and Joost van de Weijer. Minegan: Effective knowledge transfer from gans to target domains with few images. In *Conference on Computer Vision and Pattern Recognition (CVPR)*, 2020. **3**
- [45] Yaxing Wang, Chenshen Wu, L. Herranz, Joost van de Weijer, Abel Gonzalez-Garcia, and B. Raducanu. Transferring gans: generating images from limited data. In *European Conference on Computer Vision (ECCV)*, 2018. **3**
- [46] Zhou Wang, Eero P Simoncelli, and Alan C Bovik. Multiscale structural similarity for image quality assessment. In *Asilomar Conference on Signals, Systems & Computers (ACSSC)*, 2003. **7**
- [47] Sanghyun Woo, Jongchan Park, Joon-Young Lee, and In So Kweon. Cbam: Convolutional block attention module. In *European Conference on Computer Vision (ECCV)*, 2018. **4**
- [48] Dingdong Yang, Seunghoon Hong, Y. Jang, T. Zhao, and H. Lee. Diversity-sensitive conditional generative adversarial networks. In *International Conference on Learning Representations (ICLR)*, 2019. **2, 5, 6, 8**
- [49] Sangdoon Yun, Dongyoon Han, Seong Joon Oh, Sanghyuk Chun, Junsuk Choe, and Youngjoon Yoo. Cutmix: Regularization strategy to train strong classifiers with localizable features. In *International Conference on Computer Vision (ICCV)*, 2019. **5**
- [50] Han Zhang, Ian J. Goodfellow, Dimitris N. Metaxas, and Augustus Odena. Self-attention generative adversarial networks. In *International Conference on Machine Learning (ICML)*, 2019. **2**
- [51] Shengyu Zhao, Zhijian Liu, Ji Lin, Jun-Yan Zhu, and Song Han. Differentiable augmentation for data-efficient gan training. In *Conference on Neural Information Processing Systems (NeurIPS)*, 2020. **3**
- [52] Zhengli Zhao, Sameer Singh, Honglak Lee, Zizhao Zhang, Augustus Odena, and Han Zhang. Improved consistency regularization for gans. In *Conference on Artificial Intelligence (AAAI)*, 2021. **5, 6, 8**
- [53] Zhengli Zhao, Zizhao Zhang, Ting Chen, Sameer Singh, and Han Zhang. Image augmentations for gan training. *arXiv preprint arXiv:2006.02595*, 2020. **3, 6**
- [54] Bolei Zhou, Agata Lapedriza, Aditya Khosla, Aude Oliva, and Antonio Torralba. Places: A 10 million image database for scene recognition. *IEEE Transactions on Pattern Analysis and Machine Intelligence*, 2017. **6, 14**
- [55] Yang Zhou, Zhen Zhu, X. Bai, Dani Lischinski, D. Cohen-Or, and Hui Huang. Non-stationary texture synthesis by adversarial expansion. In *ACM Transactions on Graphics (TOG)*, 2018. **3**

Supplementary Material

This supplementary material is structured as follows:

- Section **A**: SIFID at different InceptionV3 layers.
- Section **B**: Ablation on the strength of the proposed diversity regularization.
- Section **C**: Effect of the proposed diversity regularization applied to comparison methods.
- Section **D**: Effect of the low-level loss $\mathcal{L}_{D_{low-level}}$.
- Section **E**: Qualitative results for the ablation study on the discriminator structure.
- Section **F**: Additional qualitative results in the Single Image and the Single Video settings.
- Section **G**: Ablation on the number of discriminator blocks used before branching.
- Section **H**: Ablation on number of channels in the layout branch feature representation.
- Section **I**: Comparison of synthesis diversity in the Single Image and Single Video settings.
- Section **J**: Analysis of strategies to generate images of rectangular shapes with different horizontal/vertical aspect ratios.
- Section **K**: Architecture and training details.

A. SIFID at different InceptionV3 layers

To evaluate image quality at different scales, we additionally compute the SIFID metric [35] at various InceptionV3 layers. Its original formulation uses InceptionV3 features before the first pooling layer, at a spatial resolution of $\frac{H \times W}{4}$. Such metric captures only low-level image details, such as colors and textures, and is not able to capture high-level semantic image properties, such as appearance of objects or global layouts. Therefore, to evaluate realism at different scales, we additionally use features before the second pooling layer (at a resolution of $\frac{H \times W}{8}$), pre-classifier features ($\frac{H \times W}{8}$) and the final Inception features (1×1), that are commonly used to compute FID [8]. To obtain the SIFID score in the Single Image setting, we generate 100 images and then compute their mean SIFID to the training image (corresponding to columns *mean* in Table 1). The results on the DAVIS-YFCC100M dataset [31, 39] for the Single Image and Single Video settings are presented in Table A and Table B.

We observe no disagreement with the metrics reported in the main paper. One-Shot GAN achieves better image quality than the comparison models in both settings,

Method	SIFID ↓			
	$\frac{H \times W}{4}$	$\frac{H \times W}{8}$	$\frac{H \times W}{16}$	1×1
SinGAN [35]	0.13	4.93	34.52	2510
ConSinGAN [9]	0.09	2.94	27.33	1960
FastGAN [24]	0.13	2.89	19.48	1340
One-Shot GAN	0.08	1.29	16.30	1100

Table A: Comparison of SIFID at different scales on DAVIS-YFCC100M in the Single Image setting.

Method	SIFID ↓			
	$\frac{H \times W}{4}$	$\frac{H \times W}{8}$	$\frac{H \times W}{16}$	1×1
SinGAN [35]	2.47	13.61	96.35	411
ConSinGAN [9]	2.74	14.73	74.50	392
FastGAN [24]	0.79	1.75	9.24	141
One-Shot GAN	0.55	1.32	5.14	115

Table B: Comparison of SIFID at different scales on DAVIS-YFCC100M in the Single Video setting.

as measured at all the InceptionV3 layers. Notably, Table A shows that single-image methods, SinGAN and ConSinGAN, achieve comparable low-level SIFID (at a resolution of $\frac{H \times W}{4}$), but achieve poor high-level scores ($\frac{H \times W}{16}$, 1×1). This indicates that these models successfully learn textures of given images, but fail to reproduce scenes at a mid-level (objects) and the global scale (layout). In contrast, our proposed two-branch discriminator allows learning the scene appearance at all scales, enabling generation of plausible images not only with fine textures, but also with correct appearance of objects and globally-coherent layouts.

B. Ablation on the strength of the proposed diversity regularization

The proposed diversity regularization (DR) is an essential component for One-Shot GAN to achieve high diversity among generated samples. For all our experiments in the main paper we used DR with $\lambda = 0.15$. In Table C, we show the effect of setting different lambdas in the Single Image setting, changing the strength of the diversity regularization. We note a general quality-diversity trade-off which is present for the Single Image setting. While diversity metrics favour diverse multi-modal outputs, the image quality metrics, such as SIFID, are computed based on similarity to the training frame, so they penalize variations from the original image [33]. We thus use SIFID at the lowest scale ($\frac{H \times W}{16}$), which corresponds to the low-level quality, such as textures, irrespective to variations in high-level patterns, such as layouts. Table C illustrates that setting the multiplier too high ($\lambda = 0.50$) leads to good diversity, but harms image quality, while setting small values ($\lambda = [0.00, 0.05]$) is beneficial for quality, but deteriorates diversity. We observed that using $\lambda = 0.15$ leads to a good trade-off, re-

DR Lambda	SIFID ↓	LPIPS ↑	MS-SSIM ↓	Pixel ↑ Diversity
0.00	0.05	0.04	0.95	0.33
0.05	0.07	0.19	0.77	0.50
0.15	0.08	0.33	0.63	0.66
0.50	0.13	0.39	0.55	0.69

Table C: Effect of the diversity regularization (DR) strength on DAVIS-YFCC100M in the Single Image setting.

sulting in a high diversity among generated samples, while not corrupting the quality of textures and the global layout coherency, so we picked this value for the final version of the model.

C. Effect of the proposed diversity regularization applied to comparison methods

To examine the effect of the proposed DR on other models, we trained SinGAN, ConSinGAN and FastGAN with the DR added to the GAN objective. Following our design, this loss was computed in the feature space, as in Eq. 3. When training the multi-stage single-image GANs from [35, 9], we applied the DR during training of each stage. To select λ_{DR} , we tested the models with the values from Table C (0.05, 0.15, 0.50), and then chose the highest coefficient that did not lead to a very high SIFID, indicating reduced low-level quality of generated images.

The performance of the models with DR, as well as our selected λ_{DR} values are included to Table D. As seen from the table, DR plays the biggest role in combination with One-Shot GAN, while applying DR to other methods leads only to minor improvement in diversity (0.01 – 0.03 MS-SSIM). For the single image GANs [35, 9] this is explained by their multi-stage training schemes: their discriminators already overfit to all possible patches at a given scale, so the DR does not help to learn more diverse combinations. Single branch discriminator of the few-shot model [24] overfits easily when trained with very little data, and DR alone cannot correct this. We conclude that our two-branch discriminator is crucial to leverage the benefit of the proposed diversity regularization.

Method	DR Lambda	SIFID ↓	LPIPS ↑	MS-SSIM ↓	Pixel ↑ Diversity
SinGAN	-	0.13	0.26	0.69	0.54
	0.15	0.15	0.26	0.68	0.55
ConSinGAN	-	0.09	0.29	0.65	0.59
	0.05	0.11	0.30	0.63	0.60
FastGAN	-	0.13	0.18	0.77	0.49
	0.15	0.14	0.21	0.74	0.52
One-Shot GAN	-	0.05	0.04	0.95	0.33
	0.15	0.08	0.33	0.63	0.66

Table D: Effect of the DR on DAVIS-YFCC100M in the Single Image setting, applied to comparison methods.

D. Effect of the low-level loss $\mathcal{L}_{D_{low-level}}$

In this section we provide an ablation on the low-level discriminator loss. According to equations 1 and 2, the loss of the two-branch discriminator is computed after each ResNet block, which means that the attention of the discriminator is shared across different layers, corresponding to image realism at different scales. Without this loss, the discriminator judges images only after branching, paying attention mostly to the high-level image realism. The low-level loss changes the discriminator’s task and shifts its attention towards earlier layers, thus increasing its ”patch” property. As seen from Table E, this property helps to reduce overfitting and allows synthesis of higher diversity, both in the Single Image and Single Video settings.

Low-level loss	Single Image		Single Video	
	SIFID ↓	LPIPS ↑	SIFID ↓	LPIPS ↑
X	0.08	0.27	0.58	0.40
✓	0.08	0.33	0.55	0.43

Table E: Ablation on the low-level loss $\mathcal{L}_{D_{low-level}}$ on DAVIS-YFCC100M dataset.

E. Qualitative results for ablations study on the discriminator structure

In Figure A and Figure B we show qualitative results for different discriminator structures. Following the ablation Table 3 in the main paper, we separately show qualitative results for our full discriminator model with content and layout branches, the discriminator without the layout branch, without the content branch, and for a model without both branches, corresponding to a standard GAN discriminator. The visual results illustrate the concepts of ”layout” and ”content” learnt by the respective branches. Applying the content branch, without the layout branch, leads to the generation of different objects in various combinations, but the model often fails to reproduce correct positioning of objects or globally-coherent layouts. For example, there might be a horizon discontinuity, or air balloons may follow unrealistically structured positions in a grid. In contrast, a model, trained with the layout branch, but without the content branch, generates images with more realistic layouts, but does not preserve the content distribution of the training image, removing objects, distorting their appearance or perturbing their shapes. Behaviour of such models corresponds to high diversity scores and poor low-level SIFID in Table 3. Applying none of the branches, which corresponds to using a standard GAN discriminator, leads to memorization of the training image, so the model just reproduces the training data (low distance to training set in Table 3). Finally, our full model with a two-branch discriminator generates plausible diverse images, varying both the image content and the

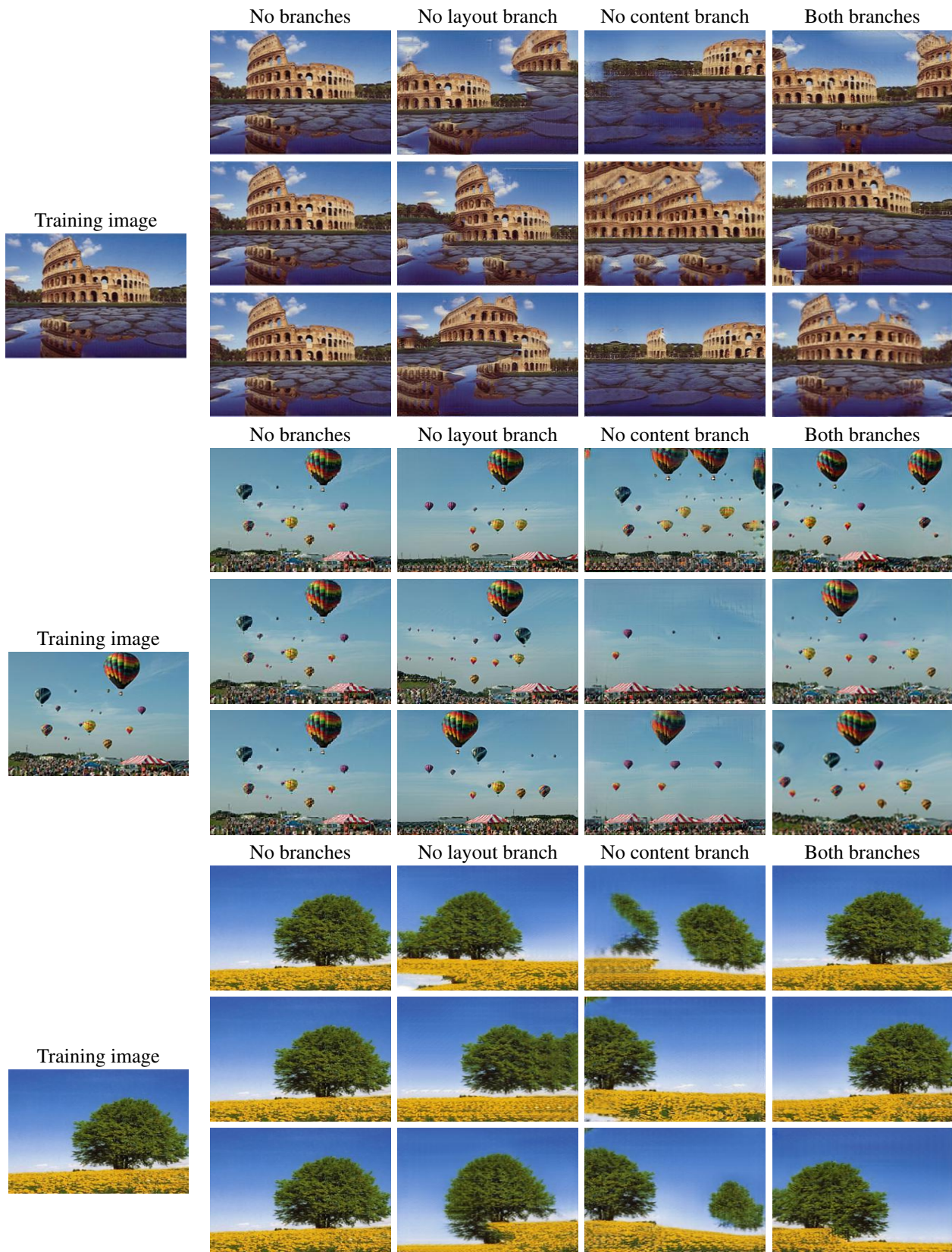


Figure A: Visual results for the ablation study on the discriminator structure. The model with a standard GAN discriminator (No branches) memorizes the training image. Model without the layout branch fails to produce images with realistic layouts or positioning of objects. Absence of the content branch does not preserve well object appearances. Finally, the model with both branches generates diverse images with realistic content and layouts. See Table 3 for qualitative comparison and Sec. E for the discussion.



Figure B: Visual results for the ablation study on the discriminator structure in the Single Video setting.

global layout of the scene (0.33 LPIPS, 0.63 MS-SSIM and SIFID at scale $\frac{H \times W}{16}$ of 16.3 in the Single Image setting).

F. Additional qualitative results in the Single Image and the Single Video settings

In Figures C, D and E we present additional qualitative results. In Figure C and Figure D we compare One-Shot GAN to other models in the Single Image setting on the Places dataset [54]. We note that the previous single-image methods, SinGAN and ConSinGAN, tend to shuffle image patches in a globally-incoherent way, as object textures may leak into surfaces of other semantic regions. Moreover, such methods do not preserve the appearance of objects, for example, by washing away sculptures in the garden or a man in the forest. For images with complex scenes these methods do not provide noticeable diversity, as in the example with a children playground. On the other hand, FastGAN [24] (see Figure D) suffers from memorization, falling into reproducing a training image or its flipped version. In contrast, our One-Shot GAN preserves objects, maintains global layout coherency and produces images with significant variability.

Figure E shows the images generated by One-Shot GAN in the Single Video setting. Compared to the Single Image setting, in this scenario there is much more data to learn from, and generative models can learn more interesting combinations of objects in the scenes. As seen from the figure, our One-Shot GAN manages to preserve the context of the training frames, at the same time adding non-trivial semantic changes to original scenes. For example, for

the shown videos, the generated frames can have a different number of balloons in sky, and combinations of planes, boats or buildings that were not seen during training.

G. Ablation on the number of discriminator blocks used before branching

The proposed One-Shot GAN has two branches, preceded by a low-level feature extractor. As discussed in Sec. 3.3, the discriminator consists of 7 stages, using 3 ResNet blocks before the branching for $D_{low-level}$, and 4 ResNet blocks for the both branches $D_{content}$ and D_{layout} . In Table F and Figure F we analyse the effect of applying branching at an earlier or a later discrimination stage, keeping the overall depth of the networks equal to 7 ResNet block. The results indicate that the branching should be applied neither too early nor too late. Using too few ResNet blocks (1-2) before the branching leads to a reduced capacity of the low-level feature extractor $D_{low-level}$, so this network becomes unable to provide the branches with descriptive content and layout representations of an image. As seen from Figure F, such model learns the color distribution of an image, but cannot produce a globally-coherent scene and generate textures of good quality. In Table F this effect is indicated by a very high SIFID. On the other hand, using too many blocks before the branching (5-6) leads to increased capacity of the feature extractor $D_{low-level}$, so the network can remember the whole image. In this case the model suffers from a memorization effect, reproducing the training image (see Figure F), and scoring low at diversity metrics (low LPIPS in Table F). Finally, we found that using 3 ResNet blocks before the

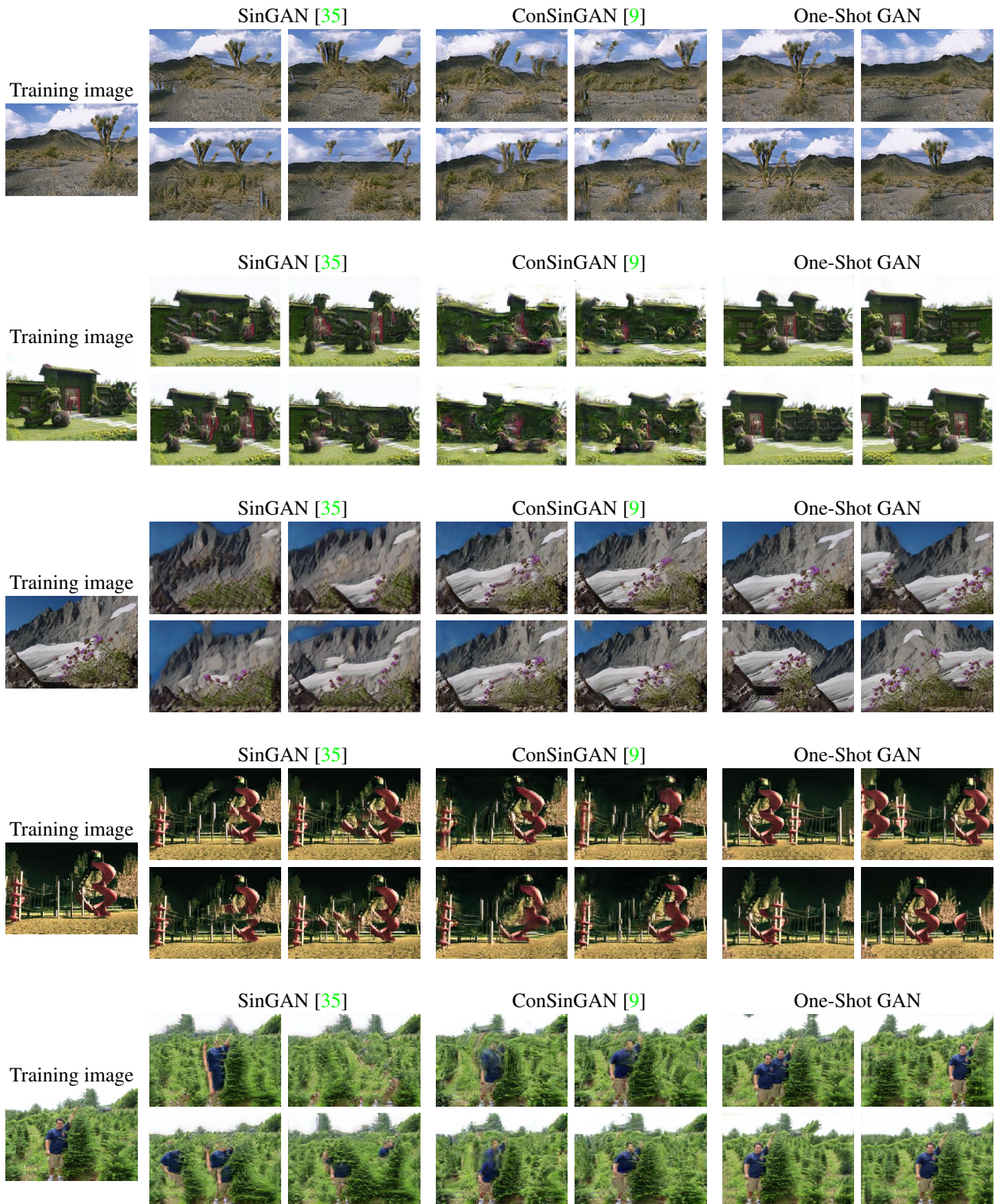


Figure C: Comparison with other methods in the Single Image setting on Places. Single-image GANs of [35, 9] are prone to incoherently shuffle image patches. In contrast, One-Shot GAN produces images preserving the appearance of objects.

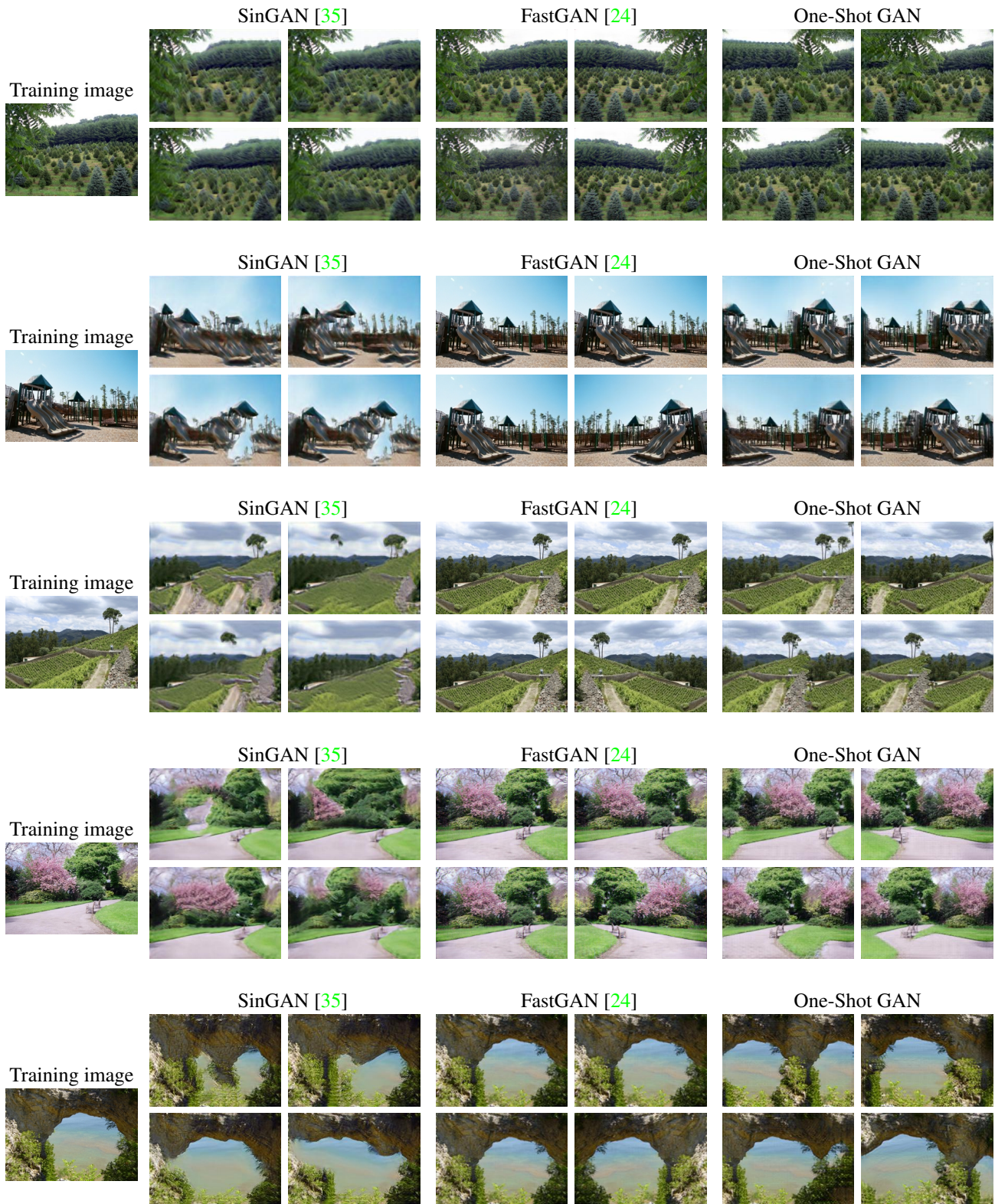


Figure D: Comparison with other methods in the Single Image setting on Places. The single-image GAN of [35] is prone to incoherently shuffle image patches, and the few-shot FastGAN model[24] reproduces the training image or its flipped version. In contrast, One-Shot GAN produces diverse images, preserving the appearance of objects.

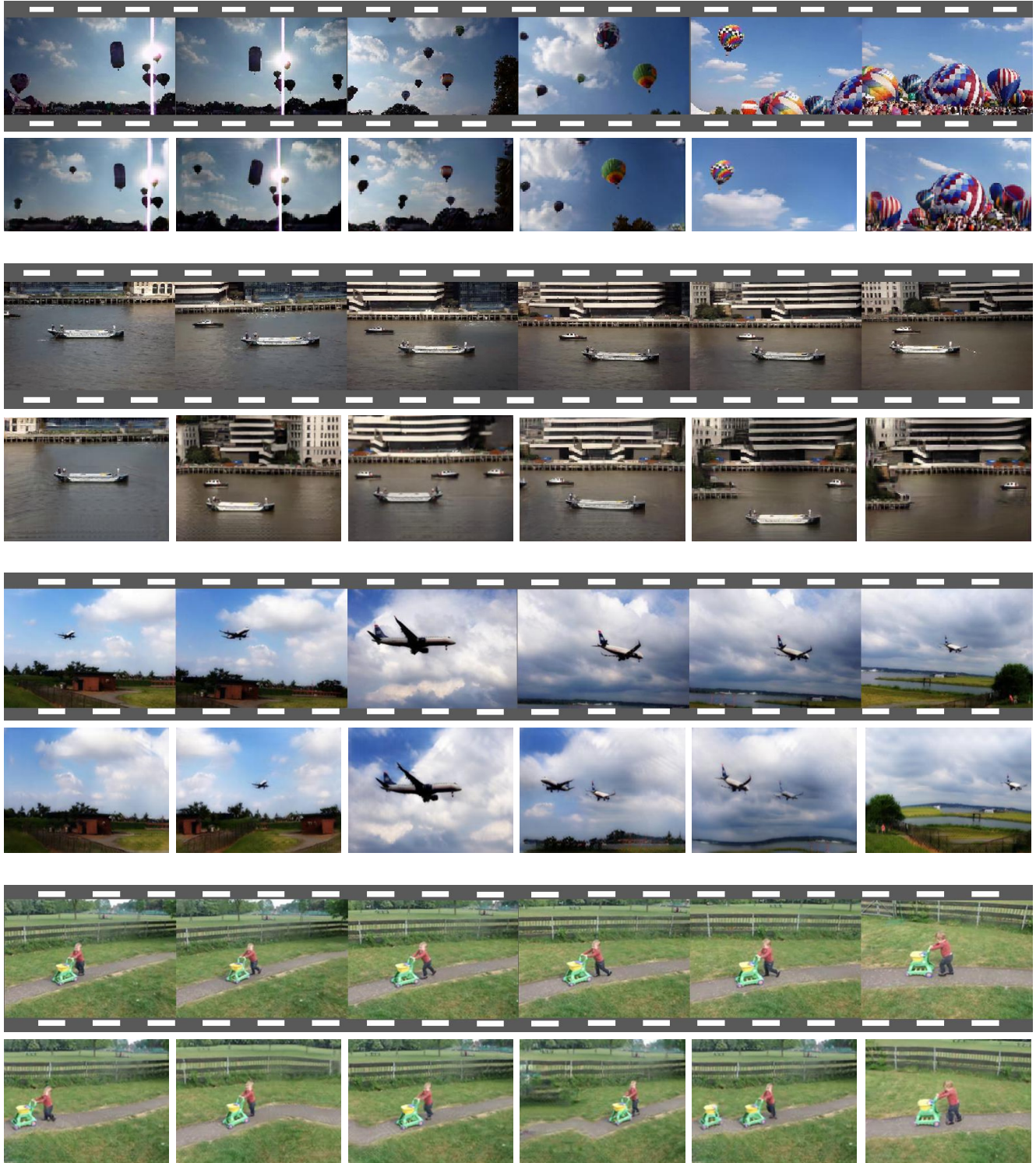


Figure E: Additional qualitative results in the Single Video setting. The training sequences are shown in grey frames. Given a single video for training, our One-Shot GAN produces images that are different to the training frames. For example, for a video with air balloons, the generated images have different number of balloons, while for a video with a boat, the model generates novel combinations of boats and buildings not seen during training.

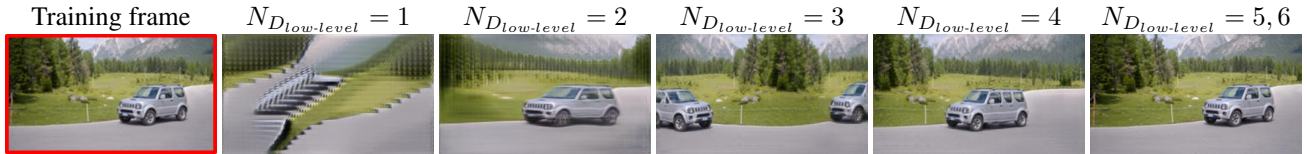


Figure F: Effect of the number of discriminator blocks used before branching. Using too few blocks (1-2) leads to reduced synthesis quality, as the $D_{low-level}$ is unable to extract the features necessary to build the content and layout representations. Increasing the number of blocks (3-4) results in improved quality while maintaining good diversity. Using too many blocks (5-6) leads to the memorization effect due to the occurring overfitting, when the model reproduces the training image with no diversity.

$N_{D_{low-level}}$	Single Image		Single Video	
	SIFID ↓	LPIPS ↑	SIFID ↓	LPIPS ↑
1	0.59	0.42	2.75	0.46
2	0.13	0.40	1.12	0.45
3	0.08	0.33	0.55	0.43
4	0.06	0.24	0.36	0.38
5	0.03	0.15	0.40	0.37
6	0.03	0.13	0.35	0.36

Table F: Ablation on the number of blocks $N_{D_{low-level}}$ in the discriminator before content-layout branching on the DAVIS-YFCC100M dataset.

branching leads to an optimal quality-diversity trade-off in both the Single Image and Single Video settings, allowing the generation of high diversity, while preserving the context of original samples.

H. Ablation on number of channels in the layout feature representation

In this section, we study the effect of varying the number of channels in the layout branch representation. For all experiments in the main paper, the layout branch representation is obtained from an intermediate representation by a convolutional layer with one output channel. Table G shows the effect of using the layout representation with 3, 5, and 10 channels. An increased number of channels in the layout branch results in a more powerful network that can easier memorize the layout representations extracted from real images. Thus, increasing the number of channels results

F_{layout} channels	Single Image		Single Video	
	SIFID ↓	LPIPS ↑	SIFID ↓	LPIPS ↑
1	0.08	0.33	0.55	0.43
3	0.07	0.28	0.54	0.41
5	0.06	0.25	0.50	0.40
10	0.06	0.24	0.49	0.40

Table G: Ablation on the number of channels used for the layout branch feature representation on the DAVIS-YFCC100M dataset.

in reduced diversity of samples, as indicated by the smaller LPIPS scores in Table G.

I. Comparison of synthesis diversity in the Single Image and Single Video settings

In Table H we compare the diversity among the images generated from a single image and from a single video on the DAVIS-YFCC100M dataset. In the Single Image setting we use only one frame in the middle of the sequence for training, while in the Single Video setting we use all video frames as training data. As seen from the table, the diversity of generated samples is notably higher for the case when all frames of a video are used (0.43 against 0.33 LPIPS). The visual difference between the settings is illustrated in Figure G. The model, trained only on the middle frame, produces slight variations of the training image. For example, such model changes the number of windows in the building or modifies the geometry of the concrete barrier. On the other hand, the model, trained on a full video, achieves more complex transformations, being capable of changing the layout of buildings or removing a person from the scene.

In practice, capturing a short video clip can take almost as little effort as collecting an image. As we show in our experiments, using short videos for training allows to generate significantly more diverse images, compared to the case when only a single image is used. This way, we would like to draw the attention of the community to the Single Video setting, which we believe to be helpful in extending the usability of generative models for practical applications.

Data setting	LPIPS ↑	MS-SSIM ↓
Single Image	0.33	0.63
Single Video	0.43	0.54

Table H: Comparison of the diversity among the images generated in the Single Image and the Single Video settings on the DAVIS-YFCC100M dataset.

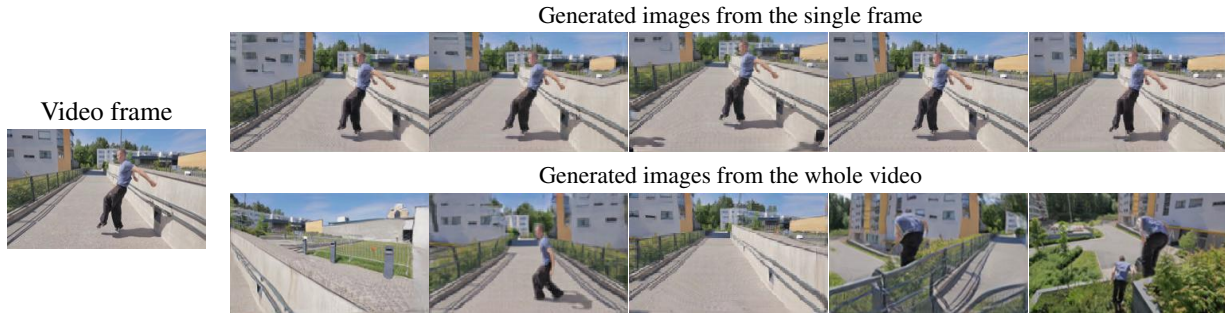


Figure G: Difference between models trained on a single middle frame of a video and on the full video sequence. In the Single Image setting, the model generates only slight geometric transformations, such as varying the number of windows on a building, or modifying the geometry of a concrete barrier. In contrast, the Single Video setting allows to provide more substantial diversity, removing the person from the frame or changing the layout of buildings.

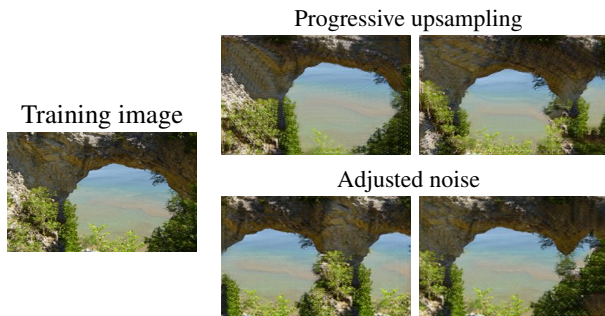


Figure H: Different strategies to achieve rectangular shapes. Using progressive upsampling, as in [35], leads to artefacts in textures (e.g. chequered “waves” on the rock). Controlling output image resolution through adjusting noise shape helps to overcome this issue and generate textures of good quality.

J. Analysis of strategies to generate images of rectangular shapes

Commonly used state-of-the-art GAN models, such as [4, 15], generate images of square shapes. In our studied settings, single images or video frames can be rectangular, having resolutions of different horizontal and vertical aspect ratios. As discussed in Sec. K, we design our model to be compatible with images of different resolutions. In this section, we analyse two possible strategies to achieve this.

One possible strategy is to follow the design of SinGAN [35], which has several training stages. Such model proposes to reach the final resolution following a geometric progression, where the image is upsampled after each training stage. In this scheme, the progression multiplier is computed based on the image size, the number of stages, and a predefined image size at first model stage. Typically, this multiplier is non-integer and is different for horizontal and vertical axes. For One-Shot GAN, we adopted such scheme by progressively upsampling the image after each

Interpolation	Single Image		Single Video	
	SIFID ↓	LPIPS ↑	SIFID ↓	LPIPS ↑
Progressive upsampling	0.11	0.32	0.65	0.42
Adjusted noise	0.08	0.33	0.55	0.43

Table I: Effect of different strategies to match the rectangular shape of the original training image on the DAVIS-YFCC100M dataset.

generator block, starting from noise of shape (4×4) and reaching the exact image shape by the final generator layers. In our experiments, such upsampling scheme leads to texture artefacts in generated images (see Figure H). We observed that the artefacts are caused by non-integer interpolation between layers: backpropagation through such transformation causes a “grid” effect, which is hard to correct during training of the generator. The difference in the texture quality in comparison to [35, 9] is explained by the fact that these models are trained in multiple stages, without requiring backpropagation through upsampling layers. In contrast, our One-Shot GAN is a single stage model, and gradients cannot bypass the interpolation.

To avoid corruptions of textures, we therefore select an alternative solution. As discussed in Sec. K, we propose to follow the architecture of [4], employing x2 upsampling after each residual block, but modifying the shape of input noise, adjusting it to fit better to the final image resolution. Note that for this approach the final resolution of generated images is an even multiple of the input noise shape, which can sometimes not precisely fit to the resolution of an original image (for example, in case when the training image has an odd number of pixels in one of the dimensions). Nevertheless, with such approach the shape of an image is preserved better, compared to generating square images as in [4, 15]. As seen from Figure H, adjusting the noise shape leads to better quality of images, overcoming the interpolation problem.

Table I confirms our analysis. We observe that using the progressive upsampling, as in [35], leads to decreased quality of images, as measured by SIFID. Moreover, such approach produces slightly lower diversity. Therefore, for our final model design, we choose to adjust input noise shape, as it leads to better performance.

K. Architecture and training details

Architecture details of our One-Shot GAN are summarized in Tables J and K. Our model has a generator G and a discriminator D consisting of three parts: low-level feature extractor $D_{low-level}$, layout branch D_{layout} , and content branch $D_{content}$. Our design mainly follows the one of BigGAN [4], applying ResNet blocks at both the generator and the discriminator. Following MSG-GAN [15], we use skip-connections between G and D . We thus generate images at different resolutions and pass them to discriminator at different scales. In contrast to [15], our discriminator is not symmetric to generator, as after $N_{low-level}$ discriminator blocks we apply branching. Therefore, we generate images only at $N_{low-level}$ highest resolutions, and then pass them at each block of $D_{low-level}$. To incorporate generated images at intermediate D blocks, we apply a 1×1 convolution, and concatenate the obtained tensor to the current D features (strategy $\phi_{lin.cat}$ from [15].)

The branches D_{layout} and $D_{content}$ are formed by usual D ResNet blocks, with two modifications. First, as the content branch has 1×1 spatial dimensions, the used convolutions have kernel size (1×1) and are technically equivalent to a fully-connected layer. Secondly, the layout branch has 1 channel, so its convolutions always have the number of channels equal to 1. To form a binary real-fake decision tensor, after each D block we use a 1×1 convolution, which maps the current features to a one-channel map with logits.

In order to fit better to the training image size, we change the resolution of the input noise. We keep the noise resolution around (4×4) , adjusting it to different ratios to fit shapes of training images closer. For example, the input noise in our experiments was resized to (3×4) , (3×5) or (4×4) , depending on the final image resolution. For evaluation, we bilinearly resized generated images to the resolution of original training image. Tables J and K present an example for input noise of resolution 3×5 , which correspond to the frames from the DAVIS video dataset [31].

We train our model with ADAM [19] optimizer, using a batch size of 5, momentums $(\beta_1, \beta_2) = (0.5, 0.999)$, learning rates 0.0002 for both the generator and the discriminator. All our experiments were conducted on a single GTX 1080 GPU with 12 GB RAM memory.

Operation	Input	Size	Output	Size
ConvTransp2D	z	(64,1,1)	up_0	(256,3,5)
ResBlock-Up	up_0	(256,3,5)	up_1	(256,3,5)
ResBlock-Up	up_1	(256,3,5)	up_2	(256,6,10)
ResBlock-Up	up_2	(256,6,10)	up_2	(256,12,20)
ResBlock-Up	up_3	(256,12,20)	up_3	(256,24,40)
ResBlock-Up	up_4	(256,24,40)	up_4	(256,48,80)
ResBlock-Up	up_5	(256,48,80)	up_5	(128,96,160)
ResBlock-Up	up_6	(128,96,160)	up_6	(64,192,320)
Conv2D, TanH	up_5	(128,48,80)	image_2	(3,48,80)
Conv2D, TanH	up_6	(64,96,160)	image_1	(3,96,160)
Conv2D, TanH	up_7	(32,192,320)	image_0	(3,192,320)

Table J: The One-Shot GAN generator. In this example, the configuration is presented for the input noise of size (3×5) and the final resolution of (192×320) , corresponding to training on the DAVIS-YFCC100M dataset in the Single Video setting.

Operation	Input	Size	Output	Size
<i>Low-level features $D_{low-level}$</i>				
Conv2D	image_0	(3,192,320)	feat_0	(32,192,320)
Conv2D	image_1	(3,96,160)	feat_1	(8,96,160)
Conv2D	image_2	(3,48,80)	feat_2	(16,48,80)
ResBlock-Down	feat_0	(32,192,320)	down_0	(64,96,160)
ResBlock-Down	down_0	(64,96,160)	down_1	(128,48,80)
	feat_1	(8,96,160)		
ResBlock-Down	down_1	(128,48,80)	F	(256,24,40)
	feat_2	(16,48,80)		
<i>Content branch $D_{content}$</i>				
AvgPool	F	(256,24,40)	F_con	(256,1,1)
ResBlock-Down	F_con	(256,1,1)	cont_0	(256,1,1)
ResBlock-Down	cont_0	(256,1,1)	cont_1	(256,1,1)
ResBlock-Down	cont_1	(256,1,1)	cont_2	(256,1,1)
ResBlock-Down	cont_2	(256,1,1)	cont_3	(256,1,1)
<i>Layout branch D_{layout}</i>				
Conv2D	F	(256,24,40)	F_lay	(1,24,40)
ResBlock-Down	F_lay	(1,24,40)	lay_0	(1,12,20)
ResBlock-Down	lay_0	(1,12,20)	lay_1	(1,6,10)
ResBlock-Down	lay_1	(1,6,10)	lay_2	(1,3,5)
ResBlock-Down	lay_2	(1,3,5)	lay_3	(1,3,5)

Table K: The One-Shot GAN discriminator. In this example, the configuration is presented for the input noise of size (3×5) and the final resolution of (192×320) , corresponding to training on the DAVIS-YFCC100M dataset in the Single Video setting.